Stabilization Method of Current Regulator for Electric Vehicle Motor Drive Systems under Motor Parameter Mismatch Conditions

Masakazu Kato
Department of Electrical engineering
Nagaoka University of Technology, NUT
Niigata, Japan
katom@stn.nagaokaut.ac.jp

Jun-ichi Itoh
Department of Electrical engineering
Nagaoka University of Technology, NUT
Niigata, Japan
itoh@vos.nagaokaut.ac.jp

Abstract— **In this paper, the stability of a current regulator for high-speed motor drives in electric vehicle is analyzed using a motor parameter mismatch model between the current regulator and actual motor parameters. As a result, a fundamental decoupling control which adds the cross terms between d-axis and q-axis to the voltage commands causes instability when the natural angular frequency of a current regulator is low under the motor parameter mismatch. The conventional method requires a low-pass filter (LPF) that has an electrical time constant in order to achieve compensation for the d-q axis coupling components. Therefore, a high carrier frequency is required in order to implement the LPF on the controller. However, it is difficult to implement the LPF because the carrier frequency is limited by the total efficiency of the motor drive systems. Therefore, this paper also proposes a stabilization method for the current regulator based on an equivalent resistance gain in order to overcome this instability problem. One of the features in the proposed method is no use of the LPF. In addition, the proposed method reduces the current overshoot by 1.1 p.u. compared with the fundamental decoupling control.**

Keywords—Interior permanent magnet synchronous motor, Induction motor, High-speed drive, Current control,

I. INTRODUCTION

In recent years, an interior permanent magnet synchronous motor (IPMSM) is actively researched in order to achieve the high efficiency in the motor drive system for electric vehicles (EV) [1]. On the other hand, a high performance induction motor (IM) is often a good choice for a low/medium-cost EV [2]. In addition, the EVs require a high-speed motor drive system in order to achieve downsizing and high output power density [3-5]. In the high speed drive region, a current regulator (ACR) becomes unstable which is caused by incomplete decoupling control for d- and q-axis cross terms due to detection delay, control delay and motor parameter errors [6]. Thereby, the dynamic decoupling control methods have been examined in order to achieve a robust ACR [7-9]. This method requires a filter which has an electrical time constant to achieve the inverse model of the motor on the decoupling controller.

However, a carrier frequency of an inverter is limited due to the efficiency [10]. As a result, the ratio of a carrier frequency (it is often same as a sampling frequency) over a synchronous frequency becomes less than ten in the high-speed motor drive systems [11]. Therefore, the LPF cannot be implemented on the ACR. Moreover, a natural angular frequency of ACR at least 10 times than that of the carrier frequency should be designed in order to achieve the stable operation of the control system. In consequence, the ratio of the synchronous frequency over the natural angular frequency of ACR becomes less than 1. In addition, the ACR of high-speed drive system generates the overshoot due to the low natural angular frequency. As a result, the output current becomes unstable and the inverter is tripped by an over current in the IPMSM drive systems. In case of the IM drive systems, this overshoot causes a torque fluctuation because the output torque is product of the torque current and the secondary flux which is generated by the d-axis current excitation current.

This paper proposes a stabilization method for the ACR for IPMSM and IM drive systems based on an equivalent resistance gain in order to overcome the instability. The proposed method does not require the LPF which has electrical time constant. The stability of decoupling control with the parameter mismatch is analyzed using the model which considers a motor parameter mismatch between the current regulator and an actual motor parameter. According to the stability analyses result, the equivalent resistance gain is designed for the drive systems. The proposed method is robust for motor parameters variations in comparison with the current regulator without the parameter error compensation.This paper is organized as follows; firstly the stability of decoupling control with the parameter mismatch for IPMSM and IM drive systems are analyzed. Secondary the proposed equivalent resistance gain is designed based on the each stability analysis. In addition, upper limit of the gain is designed consider the detection delay. Thirdly, the simulation results of IPMSM and IM drive systems are shown in order to confirm the effect of the equivalent resistance gain for the stabilization. Finally, the experimental results of the IPMSM drive system are shown in order to verify the availability of the proposed method.

II. ANALYSIS OF CURRENT CONTROL SYSTEM FOR IPMSM

A. Transfer Function of Fundamental Decoupling Control

Fig. 1 illustrates a block diagram of current control system with a fundamental decoupling control for an IPMSM. Note that the d-axis is defined as the direction of the flux vector by the permanent magnet and the direction of the q-axis is defined as the electromotive force vector. In addition, in this paper, the stability is analyzed in the continuous system shown in Fig.1 under an assumption that the discretization error can be ignored by the discretization error compensation method [11]. The IPMSM has cross terms between d- and q-axis. The current controller could be regard the cross terms as a disturbance if the motor were modeled as RL load. In order to eliminate the cross terms, a fundamental decoupling control adds the cross terms to the voltage commands of the d- and q-axis as shown in Fig.1. In the ACR has no parameter errors, the open-loop transfer functions between current command and output current become simple integral elements. Note that the proportional gain and integral gain is designed to be a first order lag response.

However, the motor parameters are varied according to temperature variation and magnetic saturation. Hence, the controller has mismatch between the ACR and the actual motor parameters. Furthermore, the mismatch results in the decoupling control error. The open-loop transfer functions which have parameter errors represented as (4) and (5). Note that in this paper, the parameters of ACR are defined as the product of the parameter error coefficients and the motor parameters.

$$G^{O}_{id\_K_{dq}}(s) = \frac{\hat{k}_{pd}s + \hat{k}_{id}}{s} P_d(s) \tag{4}$$

$$G^{O}_{iq\_K_{dq}}(s) = \frac{\hat{k}_{pq}s + \hat{k}_{iq}}{s} P_q(s) \tag{5}$$

where,

$$\hat{k}_{pd} = \omega_c K_{Ld} L_d,\ \hat{k}_{pq} = \omega_c K_{Lq} L_q,\ \hat{k}_{id} = \hat{k}_{iq} = \omega_c K_R R \tag{6}$$

$$\hat{R} = K_R R,\ \hat{L}_d = K_{Ld} L_d,\ \hat{L}_q = K_{Lq} L_q \tag{7}$$

$$P_d(s) = \frac{L_q s^2 + \left(R + \hat{k}_{pq}\right)s + \hat{k}_{iq}}{\left(R + sL_d\right)\left\{L_q s^2 + \left(R + \hat{k}_{pq}\right)s + \hat{k}_{iq}\right\} - \Delta_{dq}\Delta_{qd}s} \tag{8}$$

$$P_q(s) = \frac{L_d s^2 + \left(R + \hat{k}_{pd}\right)s + \hat{k}_{id}}{\left(R + sL_q\right)\left\{L_d s^2 + \left(R + \hat{k}_{pd}\right)s + \hat{k}_{id}\right\} - \Delta_{dq}\Delta_{qd}s} \tag{9}$$

$$\Delta_{dq} = -\omega_{re} L_q \left(1 - K_{Lq}\right) \tag{10}$$

$$\Delta_{qd} = \omega_{re} L_d \left(1 - K_{Ld}\right) \tag{11}$$

R is the armature winding resistance, L_d and L_q are the d- and q-axis components of the armature self-inductance, ω_{re} is the motor speed in electric angler frequency, ω_c is the natural angular frequency of the ACR, k_{pd} and k_{pq} are proportional gains of ACR, k_{id} and k_{iq} are integration gains of ACR, K_R is the error coefficient of armature winding resistance in the ACR. K_{Ld} and K_{Lq} are the error coefficients of the armature self- inductances. In addition, in case of the error coefficient is equal to 1, the ACR has no parameter errors. Thus, the open-loop transfer functions which has parameter errors could not maintain the simple integral characteristic due to the decoupling control error Δ_{dq} and Δ_{qd}.

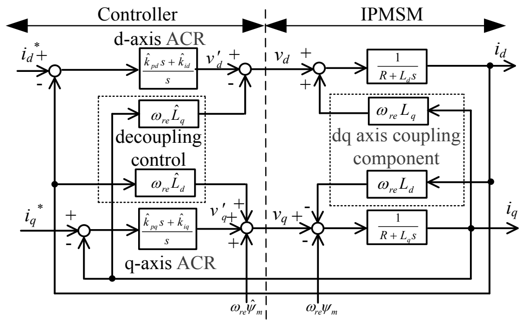

Fig. 1. Block diagram of current control system with fundamental decoupling control for IPMSM. Note that the stability is analyzed in the continuous system under an assumption that the discretization error can be ignored by the discretization error compensation method [11].

The crossed loop transfer function of Fig.1 is represented as the following equation.

$$\begin{bmatrix} i_d \\ i_q \end{bmatrix} = \begin{bmatrix} G_d(s) & -F_{dq}(s) \\ -F_{qd}(s) & G_q(s) \end{bmatrix} \begin{bmatrix} i_d^{*} \\ i_q^{*} \end{bmatrix} \tag{12}$$

where,

$$G_d(s) = \frac{b_4 s^3 + b_3 s^2 + b_2 s + b_1}{s^4 + a_4 s^3 + a_3 s^2 + a_2 s + a_1} \tag{13}$$

$$F_{dq}(s) = \frac{c_3 s^2 + c_2 s}{s^4 + a_4 s^3 + a_3 s^2 + a_2 s + a_1} \tag{14}$$

$$G_q(s) = \frac{d_4 s^3 + d_3 s^2 + d_2 s + d_1}{s^4 + a_4 s^3 + a_3 s^2 + a_2 s + a_1} \tag{15}$$

$$F_{qd}(s) = \frac{e_3 s^2 + e_2 s}{s^4 + a_4 s^3 + a_3 s^2 + a_2 s + a_1} \tag{16}$$

$$\begin{aligned} a_4 &= \frac{L_d\left(R + \hat{k}_{pq}\right) + L_q\left(R + \hat{k}_{pd}\right)}{L_d L_q}, \\ a_3 &= \frac{\left(R + \hat{k}_{pd}\right)\left(R + \hat{k}_{pq}\right) + \hat{k}_{iq}L_d + \hat{k}_{id}L_q - \Delta_{dq}\Delta_{qd}}{L_d L_q}, \\ a_2 &= \frac{\hat{k}_{id}\left(R + \hat{k}_{pq}\right) + \hat{k}_{iq}\left(R + \hat{k}_{pd}\right)}{L_d L_q}, a_1 = \frac{\hat{k}_{id}\hat{k}_{iq}}{L_d L_q} \end{aligned} \tag{17}$$

$$\begin{aligned} b_4 &= \frac{\hat{k}_{pd}}{L_d},\ b_3 = \frac{\hat{k}_{pd}\left(R + \hat{k}_{pq}\right) + \hat{k}_{id}L_q}{L_d L_q}, \\ b_2 &= \frac{\hat{k}_{pd}\hat{k}_{iq} + \hat{k}_{id}\left(R + \hat{k}_{pq}\right)}{L_d L_q},\ b_1 = \frac{\hat{k}_{id}\hat{k}_{iq}}{L_d L_q} \end{aligned} \tag{18}$$

$$c_3 = \frac{\hat{k}_{pq}\Delta_{dq}}{L_d L_q},\ c_2 = \frac{\hat{k}_{iq}\Delta_{dq}}{L_d L_q} \tag{19}$$

$$d_4 = \frac{\hat{k}_{pq}}{L_q},\ d_3 = \frac{\hat{k}_{pq}\left(R+\hat{k}_{pd}\right)+\hat{k}_{iq}L_d}{L_d L_q},$$
$$d_2 = \frac{\hat{k}_{pq}\hat{k}_{id}+\hat{k}_{iq}\left(R+\hat{k}_{pd}\right)}{L_d L_q},\ d_1 = \frac{\hat{k}_{id}\hat{k}_{iq}}{L_d L_q} \tag{20}$$

$$e_3 = \frac{\hat{k}_{pd}\omega_{re}L_d\left(1-K_{Ld}\right)}{L_d L_q},\ e_2 = \frac{\hat{k}_{id}\omega_{re}L_d\left(1-K_{Ld}\right)}{L_d L_q} \tag{21}$$

B. Unstable condition of Current Control System

From (13), the coefficients of the characteristic equation a_1, $a_2$and a_4 are positive value irrespective of the motor parameters, the parameter errors and the natural angular frequency of ACR. However, the coefficient a_3 becomes negative due to the motor parameter errors. As a result, this current control system becomes unstable with the parameter errors. The unstable condition is obtained by (22).

$$\frac{R^2}{\omega_{re}{}^2 L_d L_q} + \frac{\omega_c}{\omega_{re}}\left\{\frac{R\left(K_R+K_{Ld}\right)}{\omega_{re}L_q} + \frac{R\left(K_R+K_{Lq}\right)}{\omega_{re}L_d}\right\} + K_{Ld}K_{Lq}\left(\frac{\omega_c}{\omega_{re}}\right)^2 + \left(1-K_{Ld}\right)\left(1-K_{Lq}\right) < 0 \tag{22}$$

Then, the first, second and third term on the left hand side are reduced when ω_{re} becomes large. Therefore, the left side fourth term becomes dominant when the ACR has the error of armature self- inductance in high-speed region. In order to simplify this equation, it is assumed $\omega_{re}L >> R$ and $K_R = 1$, then the unstable condition is given by (23).

$$K_{Lq} > \frac{1}{1-\left(\frac{\omega_c}{\omega_{re}}\right)^2 \frac{K_{Ld}}{1-K_{Ld}}} \tag{23}$$

Fig. 2 shows the unstable condition of current control system with the parameter errors. Note that the parameter errors are small when the horizontal and vertical axis values in Fig.1 are close to the origin, and large when the values are far from the origin. According to the unstable condition (23), in case that the parameter error coefficients K_{Ld} and K_{Lq} are placed on the right side of each curved lines determined by the ratio of the synchronous frequency over the natural angular frequency of ACR ω_c/ω_{re}, the current control system is unstable. For example, when the error coefficients are placed on Point C ($K_{Ld} = 0.7$, $K_{Lq} = 2.0$) and the ratio ω_c/ω_{re} is 0.5, the system is stable. On the other hand, when the error coefficients are placed on Point B ($K_{Ld} = 0.6$, $K_{Lq} = 2.0$), the system becomes unstable.

Table 1 shows the motor parameters that are used in the stability analysis. Fig. 3 shows the placement and tracking of roots of the current control system with the parameter mismatch. Fig. 3 (a) shows the root loci under the condition that the error coefficients are placed on Point D ($K_{Ld} = 0.8$, $K_{Lq} = 2.0$), and

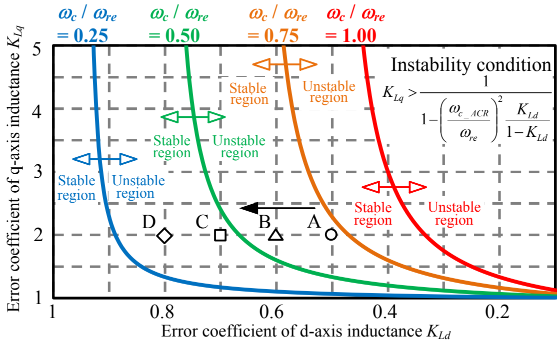

Fig. 2. Unstable condition of current control system with parameter mismatches. When the motor parameter mismatches condition is placed on the right side of each line ω_c / ω_{re}, the system is unstable.

Table 1. Parameters of test PMSM.

Rated power	3 kW
Maximum speed	12000 r/min
Pole number	4
Maximum torque	8 Nm
Rated current	24.5 A
d-axis inductance L_d	2.04 mH
q-axis inductance L_q	2.24 mH
Linked flux ψ_m	0.1066 Vs/rad
Winding resistance R	0.133 Ω
ACR natural frequency ω_c	500 rad/s (This value is determined to be half of the motor speed ω_{re}. Moreover, the condition ω_c / ω_{re} = 0.5 is comparable with the conditions ω_{re} = 15000r/min, P_f = 12 and ω_c = 4700rad/s.)

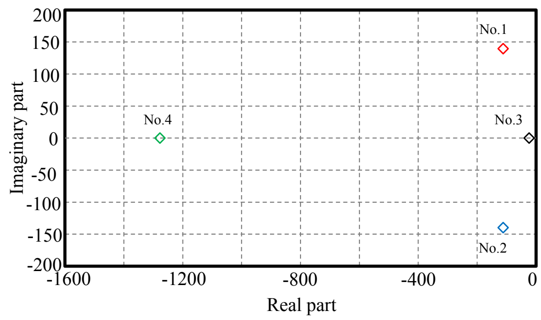

(a) Placement of four roots.

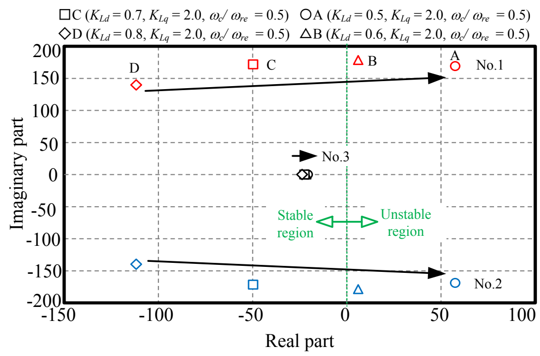

(b) Roots locus of No. 1-3.

Fig. 3. Placement and tracking of roots. The roots move into the right half plane when the error coefficients K_{Ld} and K_{Lq} increase. Each curved line determined by ω_c/ω_{re} shown in Fig.2 corresponds with imaginary axis in

ω_c/ω_{re} = 0.5. The crossed loop transfer function (11) gives the root loci of the current control system. This system has four roots, because the system is fourth -order system. The roots No. 1-3 are located nearest to the imaginary axis. Therefore, the stability of the system is discussed based on the roots No. 1-3. Fig. 3 (b) shows the roots No. 1-3 locus with the variations in K_{Ld} and K_{Lq}. The roots move into the right half plane when the error coefficients K_{Ld} and K_{Lq} increase. In particular, when the condition of error coefficients changes from Point C to B, the roots move into the right half plane. According to the above results, each curved line is determined by ω_c/ω_{re} shown in Fig.2 corresponds with the imaginary axis in complex place.

Fig. 4 shows the closed-loop frequency response of the transfer functions $G_q(s)$ and $F_{qd}(s)$. From the frequency response of the $G_q(s)$, since the error coefficients K_{Ld} and K_{Lq} increase, the bandwidth of current regulator is widened. However, the maximum gain value is increased with the increase of the error coefficients. Moreover, the current control system becomes unstable when the error coefficients K_{Ld} = 0.6 and K_{Lq} = 2.0. From the frequency response of the $F_{qd}(s)$, the maximum gain value is also increased with the increase of the error coefficients. In particular, the maximum gain is 18.3 dB at the operation point D shown in Fig. 3(b) in spite of the stable condition. Thereby, even if the d-axis current command is zero, an excessive current flows through the motor by the q-axis current command. The excessive current is the cause of an inverter trip due to an overcurrent.

III. ANALYSIS OF CURRENT CONTROL SYSTEM FOR IM

A. Characteristic Equation of Current control System

Fig. 5 illustrates a block diagram of current control system with the fundamental decoupling control for an IM which is driven by a field-oriented control. Here, the back EMF is assumed to be canceled by the feedforward compensation term. From Fig. 5 and (12), the characteristic equation of the current control system for IM is expressed by (24). In this case, the d-axis PI gains k_{pd1} and k_{id1} are set to the same value as the q-axis PI gains k_{pq1} and k_{iq1} respectively because each plant of the PI controller is same. Then, PI gains of d-, q-axis are defined as k_{p1} and k_{i1}.

$$\left(\sigma L_1 s^2 + \left(R_1 + \hat{k}_{p1}\right)s + \hat{k}_{i1}\right)^2 + \omega_{re}{}^2 \sigma L_1{}^2 \left(1 - K_\sigma K_{L1}\right)^2 \cdot s^2 = 0 \tag{24}$$

where,

$$\hat{\sigma} = K_\sigma \sigma = 1 - \frac{\hat{M}^2}{\hat{L}_1 \hat{L}_2} \tag{25}$$

$$\hat{L}_1 = K_{l1} l_1 + K_M \hat{M}, \hat{L}_2 = K_{l2} l_2 + K_M \hat{M}, \hat{M} = K_M M \tag{26}$$

$$k_{p1} = \omega_c K_{L1} L_1,\ k_{i1} = \omega_c K_{R1} R_1 \tag{27}$$

R_1 is the primary winding resistance, R_2 is the secondary winding resistance, L_1 is the primary self-inductance, L_2 is the self-inductance, M is the mutual inductance σ is the leakage coefficient, and K_{l1} , K_{l2}, K_M are error coefficients.

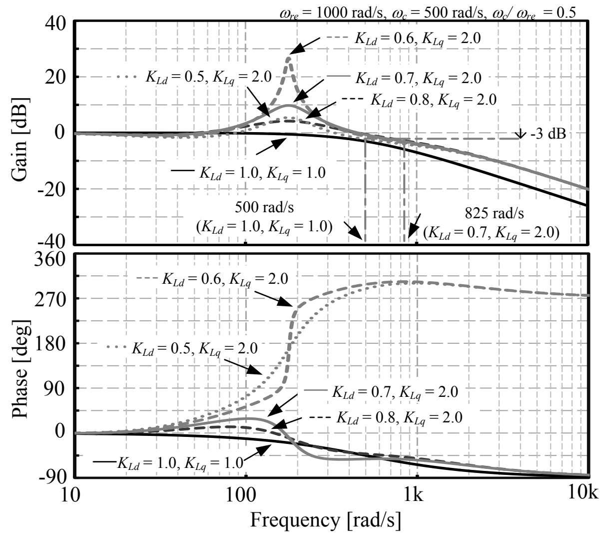

(a) Closed-loop frequency response of G_q at ω_c/ω_{re}=0.5.

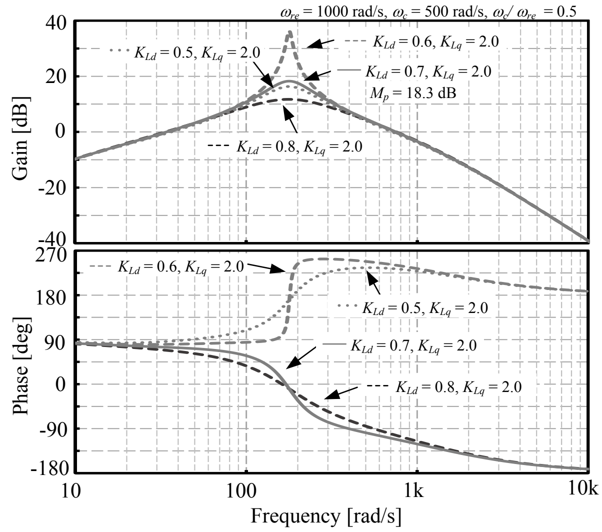

(b) Closed-loop frequency response of F_{qd} at ω_c/ω_{re}=0.5.

Fig. 4. Closed-loop frequency response of the transfer functions $G_q(s)$ and $F_{qd}(s)$ based on Fig.1. The maximum gain of $F_{qd}(s)$ is 18.3 dB at the operation point D shown in Fig. 3(b) in spite of the stable condition.

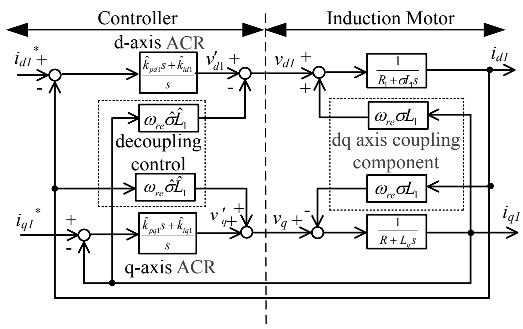

Fig. 5. Block diagram of current control system with fundamental decoupling control for IM. Here, the back EMF is assumed to be canceled by the feedforward compensation term.

The first term on the left hand side of (24) is the characteristic equation when the current control system has no parameter errors. On the other hand, the second term on the left hand side of (24) is the error term of the decoupling control.

Table 2 shows the motor parameters of the IM that are used in the stability analysis. Fig. 6 shows the roots locus based on (24) with the variations in K_{l1}, K_{l2} and K_M. In addition, the ratio ω_c/ω_{re} is 0.5. Note that the error coefficients K_{l1}, K_{l2} and K_M are assumed to same value K. Each of the parameter error coefficient is varied $K = 2.5$ from each of the no parameter error values. In order to stabilize the system, the roots should be located in the area negatively distant from the imaginary axis. The roots No.3 and No.4 move to the left side from the imaginary axis when the error coefficients increase. In contrast, the roots No.1 and No.2 approach the imaginary axis when the error coefficients increase. Therefore, the stability of the system is discussed based on the roots No.1, and No.2.

B. Stability Analysis using Approximation

Equation (24) shows the 4th order of the state equation that is complicated to evaluate the stability. In order to simplify this equation, it is assumed that there is a sufficient distance between No.3, No.4 and No.1, No2 by the large parameter errors, then (24) can be approximated as the 2nd order state equation as (28).

$$\left[2L_aK_{idq}+\left(R_a+K_{pdq}\right)^2+\omega_{re}{}^2L_a{}^2\left(1-K_{La}\right)^2\right]s^2 + 2\left(R_a+K_{pdq}\right)K_{idq}s+K_{idq}{}^2=0 \tag{28}$$

Fig. 7 shows a comparison between the 4th order model based on Fig.5 and the approximate model roots locus. Note that Fig. 7 shows the roots No. 1, 2 locus shown in Fig. 6. From Fig. 7, the roots of the approximate model is similar to the 4th order model when the error coefficient is large. Thus, the approximated model (28) is valid for the modeling of the l4th order model of current control system for IM with the output the parameter error. In order to introduce the damping factor ζ, the variables of (28) compared with the characteristic equation of the second order system is given by (29).

$$s^2+2\zeta\omega_n s+\omega_n{}^2=0 \tag{29}$$

Then, the damping factor ζ and the natural angular frequency ω_n is expressed as (30).

$$\zeta=\frac{R_1+k_{p1}}{\sqrt{2k_{i1}\sigma L_1+\left(R_1+k_{p1}\right)^2+\omega_{re}{}^2\sigma^2L_1{}^2\left(1-K_\sigma K_{L1}\right)^2}} \tag{30}$$

$$\omega_n=\frac{k_{i1}}{\sqrt{2k_{i1}\sigma L_1+\left(R_1+k_{p1}\right)^2+\omega_{re}{}^2\sigma^2L_1{}^2\left(1-K_\sigma K_{L1}\right)^2}} \tag{31}$$

According to (30), ζ and ω_n become small when the error coefficient is large. Hence, the system becomes unstable.

IV. Proposed Method for Stabilization of System

A. Esuivalent Registance Gain for Stabilization of Current Control System

Fig. 8 shows the block diagram of the current regulator with the equivalent resistances k_r. In order to increase the armature winding resistance R, the product of detection current and k_r is substracted from the inverter voltage command v^*. In consequence, the armature winding resistance becomes equivalent to the sum of R and k_r. In the IPMSM, depending on the increase of the armature winding resistance, the first, second

Table 2. Parameters of test IM.

Pole number	4
Primary resistance R_1	0.414 Ω
Secondary resistance R_2	0.423 Ω
Primary leakage inductance l_1	1.24 mH
Secondary leakage inductance l_2	1.24 mH
Mutual inductance M	34.5 mH

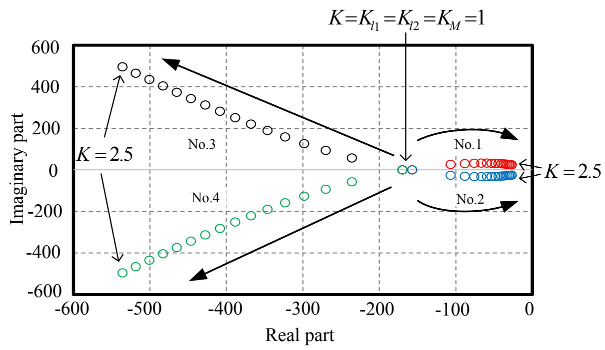

Fig. 6. Roots locus with variations in K_{l1}, K_{l2} and K_M. Note that the error coefficients are assumed to same value. Each of the parameter error coefficient is varied $K = 2.5$ from each of the no parameter error values.

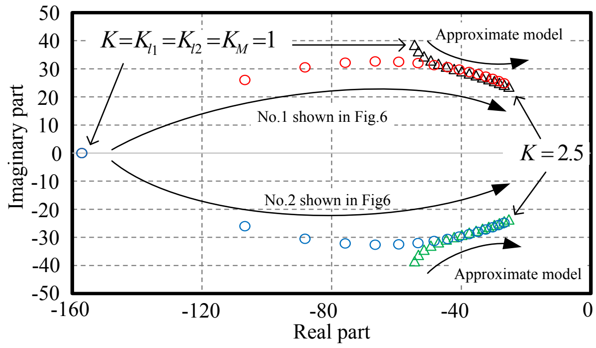

Fig. 7 Comparison between the 4th order model and the approximate model roots locus. Note that Fig. 7 shows the roots No. 1, 2 locus shown in Fig. 6.

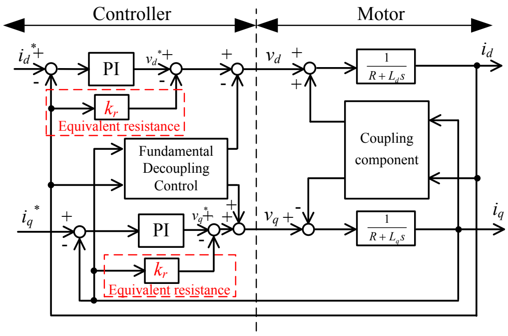

Fig. 8. Block diagram of current regulator with equivalent resistances. The armature winding resistance becomes equivalent to the sum of R and k_r. The unstable phenomenon of current regulator is preventable by k_r in the high speed region.

and third term on the left hand side of (2) are increased. In addition, in the IM, the first term on the left hand side of (24) is increased. Therefore, the unstable phenomenon is preventable by additional gain k_r in the high speed region. Note that the proposed method does not require the LPF which has electrical time constant. Therefore, the proposed method can be applied to the high-speed drive systems.

B. Equivalent Registance Gain Design for IPMSM

Fig. 9 shows the transition of the root locus with the proposed method when the gain k_{r_PM} is gradually changed. At the equivalent resistance gain $k_{r\_PM} = 0$, the poles are placed on the right half plane. By contrast, when the equivalent resistance gain k_r increases, the poles move into left half plane. In order to define the lower limit of k_{r_PM},it is necessary to solve the condition in which the coefficient a_3 becomes positive value. The lower limit is derived from (22) in consideration of equivalent resistance. Then, the lower limited is given by (32).

$$k_{r\_PM} > \frac{-K_1 + \sqrt{K_1^2 - 4K_2}}{2} - R \tag{32}$$

where,

$$K_1 = \omega_{re}\left(K_{Ld}L_d + K_{Lq}L_q\right) \tag{33}$$

$$K_2 = K_R R\left(L_d + L_q\right) + L_d L_q\left\{K_{Ld}K_{Lq} + \omega_{re}^2\left(1-K_{Ld}\right)\left(1-K_{Lq}\right)\right\} \tag{34}$$

Fig. 10 shows the block diagram of q-axis current control system with a detection delay. Table 3 shows the Routh table of the current control system with the detection delay shown in Figure 5. Note that the dead time is approximated by first-order Pade approximation. The value of k_{r_PM} is limited by the detection delay because β_1 becomes negative due to the increase of k_r. In order to derive this equation, it is assumed $T_d\ T_f \cong 0$. Then, the upper limit of k_{r_PM} is obtained by (35).

$$k_{r\_PM} < \frac{2L_q\left(T_d + 2T_f\right)}{T_d\left(T_d + 4T_f\right)} \tag{35}$$

C. Equivalent Resistance Gain Design for IM

Fig. 11 shows the transition of the root locus with the proposed method when the gain k_{r_IM} is gradually changed. At the equivalent resistance gain $k_{r\_IM} = 0$, the poles are placed on close to the imaginary axis. On the other hand, when the equivalent resistance gain k_r increases, the poles move the left side from the imaginary axis. In order to derive the k_{r_IM}, it is necessary to solve (30) for R_1. The k_{r_IM} is derived from (30) in consideration of equivalent resistance, as given by

$$k_{r\_IM} > \frac{-K_3 - \sqrt{K_3^2 - 4K_4}}{2} \tag{36}$$

where,

$$K_1 = 2\left\{\omega_c L_a \zeta^2 + \left(R_a + K_{pdq}\right)\left(\zeta^2 - 1\right)\right\} \tag{37}$$

$$K_2 = \left(R_a + K_{pdq}\right)^2\left(\zeta^2 - 1\right)^2 + \left\{\omega_{re}^2 L_a^2\left(1 - K_{La}\right)^2 + 2\omega_c L_a K_R R\right\}\zeta^2\left(\zeta^2 - 1\right) \tag{37}$$

Note that the upper limit of k_{r_IM} is the same as (35).

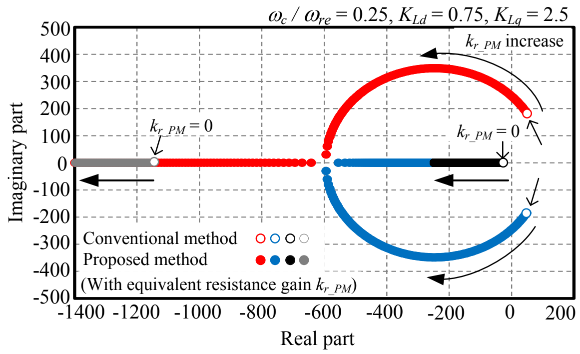

Fig. 9. Root locus with proposed method. The poles of conventional method are placed on the right half plane. By contrast, when the equivalent resistance gain k_r increases, the poles move into left hand place.

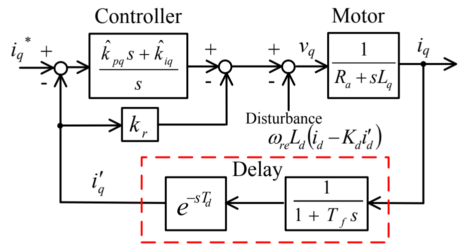

Fig. 10. Block diagram of q-axis current control system of proposed method with a detection delay. The detection delay of the control system is approximated by dead time and time constant of a first-order lag system.

Table 3. Routh table of the current control system with the detection delay shown in Fig. 5. Note that the dead time is approximated by first-order Pade approximation.

s^4	$\alpha_1 = L_q T_f \frac{T_d}{2}$	$\alpha_2 = R_a\left(T_f + \frac{T_d}{2}\right) + L_q - \frac{T_d}{2}\left(K_{pq} + k_{rq}\right)$	$\alpha_0 = K_{iq}$
s^3	$\alpha_3 = R_a T_f \frac{T_d}{2} + L_q\left(T_f + \frac{T_d}{2}\right)$	$\alpha_1 = R_a + k_{rq} + K_{pq} - \frac{T_d}{2}K_{iq}$	0
s^2	$\beta_1 = \frac{\alpha_3\alpha_2 - \alpha_4\alpha_1}{\alpha_3}$	$\beta_2 = \frac{\alpha_3\alpha_0}{\alpha_3}$	0
s^1	$\gamma_1 = \frac{\beta_1\alpha_1 - \alpha_3\beta_2}{\beta_1}$	0	0
s^0	α_0	0	0

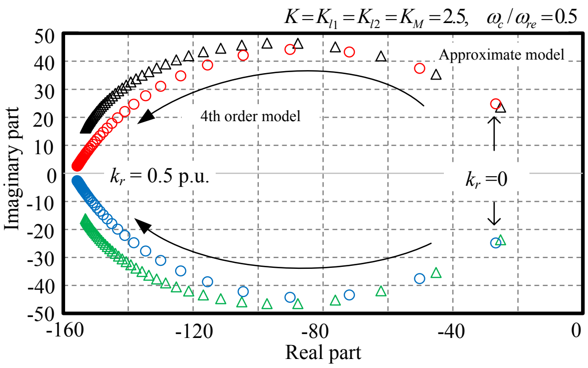

Fig. 11 Root locus with proposed method when the gain k_{r_IM} is gradually changed. When the equivalent resistance gain k_r increases, the poles move to the left side from the imaginary axis.

V. Simulation and Experimental Results

A. Simulation Results

Fig. 12 shows an output d-q axis current response with and without the proposed method. Fig. 12 (a) shows the results of the step response for the IPMSM under the conditions $K_d = 0.7$, $K_q = 2.0$, $\omega_c / \omega_{re} = 0.5$, (b) shows the results of the step response for the IM under the conditions $K_{I1}=K_{I2}=K_M=2.5$, $\omega_c / \omega_{re} = 0.5$. IN Fig.12 (a), an output current overshoot of the system without the proposed method is 230%. In addition, the peak value of the output current is 3.3 times large as rated current of test motor. In this case, in order to prevent the motor and drive circuit such as inverter from breakdown, the drive circuit is tripped. In controast, the proposed method reduces the d-, q-axis current overshoots by 230% because of the proposed equivalent resistance gain in comparison with the conventional method. Hence, it is confirmed that the proposed method achieves no overshoot of the output current in the simulations. In Fig.12 (b), the system without the proposed method generates a d-axis current overshoot of 105%. This overshoot causes a torque fluctuation because the output torque of IM is product of the q-axis current (torque current) and the secondary flux which is generated by the d-axis current (excitation current). On the other hand, the proposed method suppress the overshoot to 30%. Furthermore, the response time correspond to the deign value. Hence, it is confirmed that the proposed method achieves less overshoot of the output current than the conventional method in the simulations.

B. Experimental Results

According to Fig.12, the stabilization method of IPMSM is more effective than that of the IM. Therefore, this paper evaluates the stability of the proposed method for IPMSM by the experiments.

Fig. 13 shows the configuration of IPMSM drive system. In order to confirm the effectiveness of the proposed method, the experiments are demonstrated with a motor - generator set shown in Fig. 13. The rated power of this motor - generator set is 3.0 kW. The test motor is IPMSM shown in Table 1.

Fig. 14 shows an output d-q axis current response with and without the proposed method. Figure 14 (a) shows the result of the conventional method under the conditions $K_d = 0.7$, $K_q = 2$, $\omega_c / \omega_{re} = 0.5$ without the proposed method, (b) shows the result with the conventional under the conditions $K_d = 0.7$, $K_q = 2$, $\omega_c / \omega_{re} = 0.5$. In Fig. 14 (a), a output current overshoot is 60%. Furthermore, the inverter is tripped by an over current. This overshoot current is due to gain characteristic of $F_{qd}(s)$ shown in Fig.4 (b). In order to avoid the inverter trip, the output torque is limited by the magnitude of the overshoot current. On the other hand, the proposed method suppresses the overshoot because the the unstable phenomenon is preventable by additional gain k_r. Moreover, the designed response is achieved with the proposed method. As a result, it is confirmed that the proposed method is robust for motor parameters variations.

Fig. 15 shows output current response with the speed control in a field-weakening control region. In Fig. 15 (a), an output current becomes unstable and the inverter is tripped by an over current. On the other hand, in the proposed method, the motor is

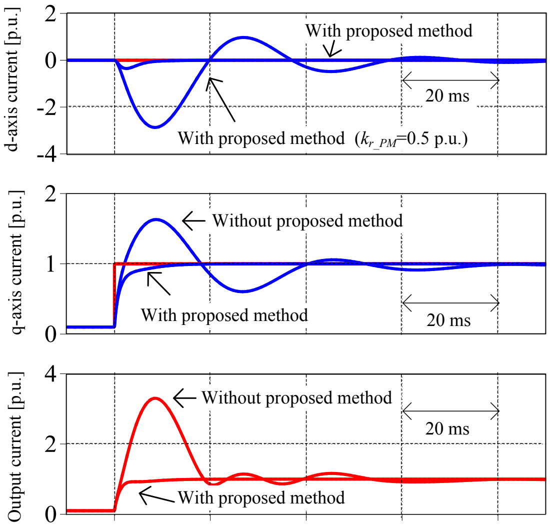

(a) IPMSM under the conditions $K_d = 0.7$, $K_q = 2.0$, $\omega_c / \omega_{re} = 0.5$ with and without proposed method an output current overshoot of the system without proposed method is 230%. In controast, the proposed method reduces the d-, q-axis current overshoots by 230%

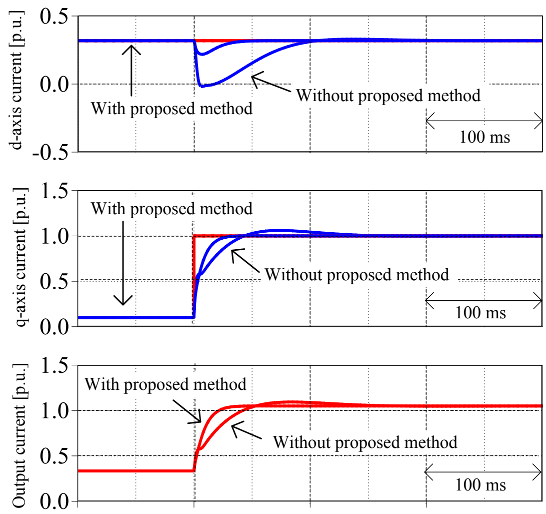

(b) IM under the conditions $K_{I1}=K_{I2}=K_M=2.5$, $\omega_c / \omega_{re} = 0.5$ with and without proposed method. The system without proposed method generates a d-axis current overshoot of 50%.

Fig. 12. Output current response with/without proposed method.

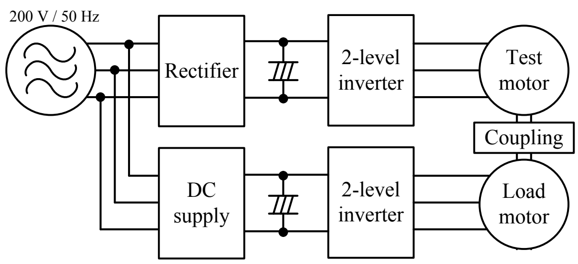

Fig. 13. Configuration of PMSM drive system. The rated power of this motor - generator set is 3.0 kW. The test motor is IPMSM shown in Table 1.

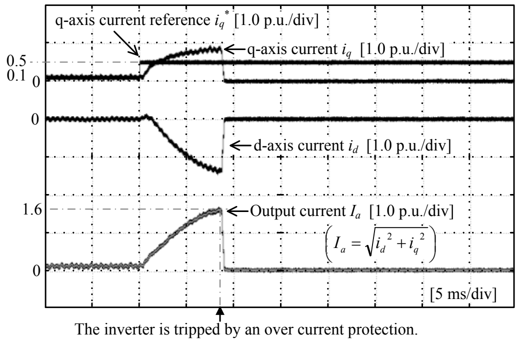

(a) Without proposed method at the condition C shown in Fig.2.
(ω_c=500 rad/s, ω_{re}/ω_c=0.5, K_d=0.7, K_q=2.0, k_r=0)

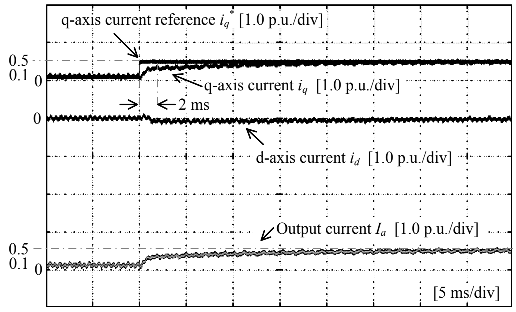

(b) With proposed method at the condition C shown in Fig.2.
(ω_c=500 rad/s, ω_{re}/ω_c=0.5, K_d=0.7, K_q=2.0, k_r=0.5)

Fig. 6. Output current response with/without proposed method. As a result, the stability is confirmed under the instability region of the fundamental decoupling control method with parameter mismatches.

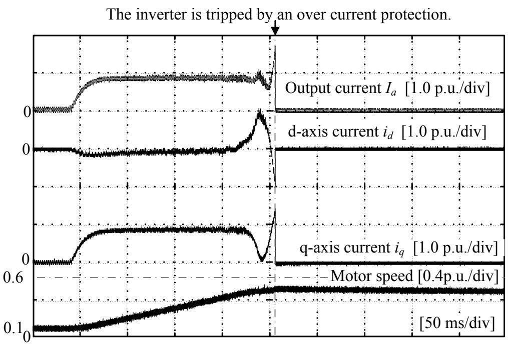

(a) Conventional method at the condition C shown in Fig.2.
(ω_c=1000 rad/s, K_d=0.7, K_q=2.0, k_r=0)

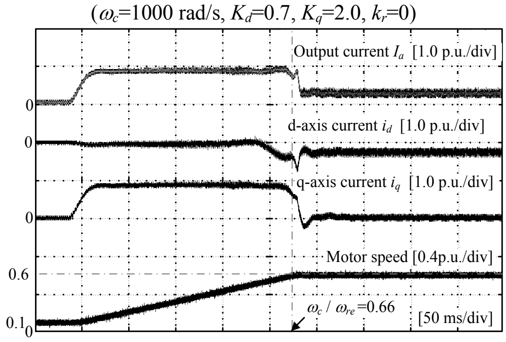

(b) Proposed method at the condition C shown in Fig.2.
(ω_c=1000 rad/s, K_d=0.7, K_q=2.0, k_r=0.5)

Fig. 7. Output current response with the speed control in a field-weakening control region. In the proposed method, the motor is accelerated to the field-weakening control region.

accelerated to the field-weakening control region without the current overshoot. As a result, the stability is confirmed under the instability region of the fundamental decoupling control method with parameter mismatch.

VI. Conclusions

This paper presents a stabilization method of the current regulator for high speed motor drives under motor parameter mismatch condition without the LPF which has electrical time constant. In order to increase the armature winding resistance R for stabilization of the motor drive systems, the product of the detection current and the equivalent resistances is substracted from the inverter voltage command.The proposed method has no output current overshoot under the instability region of the fundamental decoupling control method. From simulation result, the proposed method suppress the overshoot of IM to 30%. Furthermore, the response time correspond to the deign value. From experimental result, the propsed method suppress the output current overshoot of IPMSM by 1.1 p.u.. Moreover, the designed response is achieved with the proposed method. As a result, it is confirmed that the proposed method is robust for motor parameters variations.

References

[1] D. Sato, J. Itoh: "Total Loss Comparison of Inverter Circuit Topologies with Interior Permanent Magnet Synchronous Motor Drive System", 5th IEEE Annual International Energy Conversion Congress and Exhibition, Vol. , No. 5-5-4, pp. 537-543 (2013)

[2] Xi Zhang, “Sensorless Induction Motor Drive Using Indirect Vector Controller and Sliding-Mode Observer for Electric Vehicles,” IEEE Transactions on Vehicular Technology, Vol. 62, No. 7, pp. 3010 - 3018 , sept 2013

[3] A. M. EL-Refaie, J. P. Alexander, S. Galioto, P. B. Reddy, K. K. Huh, P. Bock, and X. Shen, “Advanced High-Power-Density Interior Permanent Magnet Motor for Traction Applications,” IEEE Transactions On Industry Applications, Vol. 50, No. 5, pp. 3235-3248 , Sep./Oct., 2014

[4] E. Sulaiman, T. Kosaka, N. Matui, “High Power Density Design of 6-Slot-8-Pole Hybrid Excitation Flux Switching Machine for Hybrid Electric Vehicles,” IEEE Trans. On Magnetics, Vol. 47, No. 10, pp. 4453-4456, Oct., 2011

[5] D. Matsuhashi, K. Matsuo, T. Okitsu, T. Ashikaga, T. Mizuno, “Comparison Study of Various Motors for EVs and the Potentiality of a Ferrite Magnet Motor,” IEEJ Journal of Industry Applications, Vol. 4, No. 4, pp. 503-511 , July 2015

[6] D. W. Novotny, and T. A. Lipo, “Vector control and dynamics of ac drives,” Oxford Science Publications, 1996

[7] J. Jung, and K. Nam, “A Dynamic Decoupling Control Scheme for High-Speed Operation of Induction Motors,” IEEE Trans. On Industrial Electronics, Vol. 46, No. 1, pp. 100-110, Feb. 1999

[8] H. Zhu, X. Xiao and Y. Li, “PI Type Dynamic Decoupling Control Scheme for PMSM High Speed Operation,” Applied Power Electronics Conference and Exposition (APEC) 2010, pp. 1736-1739, Feb. 2010

[9] Yukihiro Yoshida, Kenji Nakamura, Osamu Ichinokura, “Quick-Response Technique for Simplified Position Sensorless Vector Control in Permanent Magnet Synchronous Motors”, IEEJ Journal of Industry Applications, Vol. 4, No. 5, pp. 582-588 , Sep. 2015

[10] Yukihiro Yoshida, Kenji Nakamura, Osamu Ichinokura, “Evaluation of Influence of Carrier Harmonics of SPM Motor Based on Reluctance Network Analysis”, IEEJ Journal of Industry Applications, Vol. 3, No. 4, pp. 304-309 , July 2014

[11] B. H. Bae, and S. K. Sul, “A Compensation Method for Time Delay of Full-Digital Synchronous Frame Current Regulator of PWM AC Drives,” IEEE Transactions On Industry Applications, Vol. 39, No. 3, pp. 802-810 , May/June 2003